

A measurement of the neutral current electroweak parameters using the Fermilab narrow band neutrino beam

P.G. Reutens^{1,2}, F.S. Merritt, M.J. Oreglia

Enrico Fermi Institute and Physics Department, University of Chicago, Chicago, IL 60637, USA

P. Auchincloss³, R.E. Blair⁴, C. Haber⁵, S.R. Mishra, E. Oltman, M. Ruiz⁶,
F.J. Sciulli, M.H. Shaevitz, W.H. Smith⁷, R. Zhu

Columbia University, New York, NY 10027, USA

R. Coleman, H.E. Fisk, B. Jin, T. Kondo, D. Levinthal⁸, W. Marsh, P.A. Rapidis,
H.B. White, D. Yovanovitch

Fermi National Accelerator Laboratory, Batavia, IL 60510, USA

A. Bodek, F. Borchering⁹, N. Giokaris¹⁰, K. Lang¹¹, I.E. Stockdale¹²

University of Rochester, Rochester, NY 14627, USA

Received 1 September 1988; in revised form 15 June 1989

Abstract. We report a measurement of the electroweak parameters $\sin^2\theta_W$ and ρ based on the ratios of neutral current to charged current events measured in the Fermilab narrow-band neutrino beam at energies of 30–240 GeV. The data are fully corrected for radiative effects, heavy-quark production, and other effects. The best value for $\sin^2\theta_W$ obtained, $\sin^2\theta_W = 0.239 \pm 0.011$, is consistent with the most recent values from W and Z production, as well as from other neutrino experiments.

Introduction

This paper presents a measurement by the CCFR group of the electroweak parameters $\sin^2\theta_W$ and ρ

¹ In partial fulfillment of the Ph.D. requirement at the University of Chicago

Present addresses:

² Yale University Law School, New Haven, Conn., USA

³ University of Rochester, Rochester, NY 14627, USA

⁴ Argonne National Laboratory, Argonne, IL 60439, USA

⁵ LBL, Berkeley, CA 94720, USA

⁶ CERN, Geneva, Switzerland

⁷ University of Wisconsin, Madison, WI 53706, USA

⁸ Florida State University, Tallahassee, FL 32306, USA

⁹ Fermilab, Batavia, IL 60510, USA

¹⁰ Rockefeller University, New York, NY 10021, USA

¹¹ Stanford University, Stanford, CA 94305, USA

¹² University of Illinois, Urbana, IL 60510, USA

using the ratio of neutral- to charged-current deep inelastic neutrino interactions. The data were taken in two Fermilab experiments, E616 and E701, both using the narrow band neutrino beam at Fermilab. Results have already been published [1] for the first of these runs (E616). The analysis [2] presented here combines both runs and more than doubles the previous event sample.

The Weinberg angle θ_W specifies the electroweak mixing in neutral current interactions. Unlike θ_W , ρ is not a fundamental parameter in the simplest Weinberg-Salam model, in which $\rho = 1$; ρ is used to specify the relative strengths of neutral and charged-current weak interactions, and is related to the structure of the Higgs sector in extended models. In this experiment, $\sin^2\theta_W$ and ρ were determined from the ratios of neutral-current (NC) to charged-current (CC) events using the equations [3]

$$R^v = \sigma_{\text{NC}}^v / \sigma_{\text{CC}}^v = \rho^2 \left(\frac{1}{2} - \sin^2\theta_W + \frac{5}{9} \sin^4\theta_W (1+r) \right) \quad (1)$$

$$R^v = \sigma_{\text{NC}}^v / \sigma_{\text{CC}}^v = \rho^2 \left(\frac{1}{2} - \sin^2\theta_W + \frac{5}{9} \sin^4\theta_W \left(1 + \frac{1}{r} \right) \right) \quad (2)$$

where $r = \sigma_{\text{CC}}^v / \sigma_{\text{CC}}^v$. These equations are valid even after cuts in $y = E_{\text{had}}/E_\nu$ are applied to both NC and CC events, provided that R^v , $R^{\bar{v}}$, and r are all evalu-

ated within the same cuts. However the equations are exact only for an idealized target, and must be corrected for the non-zero charmed-quark mass, radiative effects, and the non-isoscalar target.

For values of $\sin^2\theta_W \approx 0.24$, $\sin^2\theta_W$ is insensitive to R^ν . The measurement of $\sin^2\theta_W$ is determined almost entirely by R^ν , and R^ν is only useful for measuring ρ .

The Fermilab narrow-band neutrino beam

The narrow-band neutrino beam was formed by targeting 400 GeV primary protons on a BeO target to produce high-energy secondary pions and kaons. These were sign- and momentum-selected by an array of quadrupoles and dipoles to produce a collimated beam with momentum spread $\Delta p/p \approx 0.10$ and angular divergence $\Delta\theta \approx 0.15$ mrad. These passed into a 350m long evacuated decay pipe where neutrinos were produced by $\mu\nu$ decays of the pions and kaons. Hadrons which did not decay were absorbed in a 6.5 m steel and aluminum beam dump at the end of the decay pipe. Muons were absorbed by 930 m of earth and steel shielding between the beam dump and the neutrino detector.

Due to two-body decay kinematics, the neutrino spectrum resulting from the decays of secondary hadrons was dominated by two bands, a high-energy band from K -decay ($E_{\max}^\nu = 0.95 E_{\text{beam}}$) and a lower-energy band from π -decay ($E_{\max}^\nu = 0.43 E_{\text{beam}}$), as shown in Fig. 1 for $E_{\text{beam}} = 200$ GeV. The neutrino energy within each band decreased as a function of increasing decay angle and therefore of increasing radius r of the event vertex as measured from the beam center in the detector, as shown in Fig. 2. This two-band structure and the ability to determine $E_\nu(r)$ from the radius of the event vertex were used in the analysis to provide information about the incident E_ν , as described below.

The data were taken in two runs, E616 (in 1979–80) and E701 (in 1982). In E616, data were taken at secondary beam settings of 120, 140, 168, 200, and 250 GeV, for both positive beam (ν) and negative beam ($\bar{\nu}$), with a total of 22744 observed charged-current ν events (after the rather stringent cuts required for the neutral current analysis). In E701, data were taken at positive beam settings of 100, 140, 165, 200, and 250 GeV, giving an additional 32280 CC events.

Backgrounds from cosmic ray interactions were a potential problem due to the unrestrictive neutral current trigger requirements. To minimize this background, the beam was extracted in the fast-spill mode for the neutrino experiment (after a slow-spill extraction for other experiments on site). For E616, the detector was live only during the fast beam spill of 1–

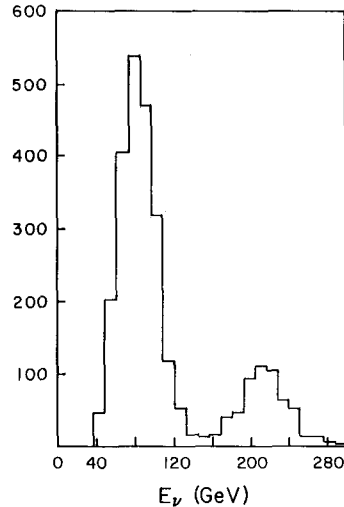


Fig. 1. The measured E_ν spectrum for the 200 GeV secondary beam

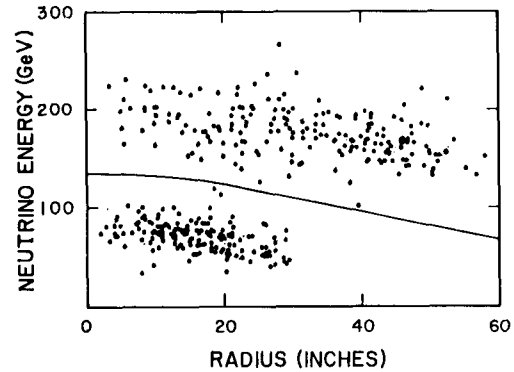


Fig. 2. Measured E_ν as a function of radius r at the detector for $E_{\text{beam}} = 200$ GeV

2 ms; in E701, in order to improve statistics while keeping the instantaneous rate and deadtime sufficiently low, beam was also extracted in five “pings” of width ≤ 1 ms each during the slow spill extraction.

A potential contamination of “wide-band background” neutrinos, produced from secondaries which decayed before momentum selection, was minimized by configuring the momentum-selecting magnets so that the beam did not point directly at the neutrino detector before the final bend. As a result, the wide band neutrino flux was small and peaked at low energies. This flux was directly measured by running with the momentum-defining collimator closed to prevent secondaries from entering the decay pipe.

The steering of the secondary beam was monitored using vertical and horizontal split-plate ion chambers in the decay pipe. These were used in the data analysis to reject beam spills in which the centroid of the neutrino beam deviated by more than ± 4 cm from its mean at the neutrino detector.

Additional beam monitors were used to measure particle ratios, beam divergence, beam energy, and flux, and are described in detail elsewhere [4]. The analysis presented here does not require normalized fluxes, since the R^ν and $R^{\bar{\nu}}$ in (1) and (2) are the ratios of neutral to charged-current events. Flux measurements enter only through parameter $r = \sigma_{CC}^{\bar{\nu}}/\sigma_{CC}^{\nu}$, which introduces a negligible error in $\sin^2\theta_W$.

The neutrino detector

The neutrino detector is shown schematically in Fig. 3. Interactions occurred in the target-calorimeter, which contained a total mass of 690 tons and consisted of $305\text{ cm} \times 305\text{ cm} \times 5\text{ cm}$ steel plates instrumented with $305\text{ cm} \times 305\text{ cm}$ liquid scintillation counters and spark chambers, with a counter after every 10 cm of steel and a chamber after every 20 cm. The calorimeter was followed by a magnetized toroidal spectrometer used to measure E_μ (for charged-current studies) with a root-mean-square resolution of $\delta E_\mu/E_\mu = 11\%$.

In the measurement of R^ν presented here, no tracking or spectrometer information was used. The spark chambers were used only to measure the transverse coordinates of the event vertex using the centroid of sparks produced in the hadron showers of both neutral- and charged-current events.

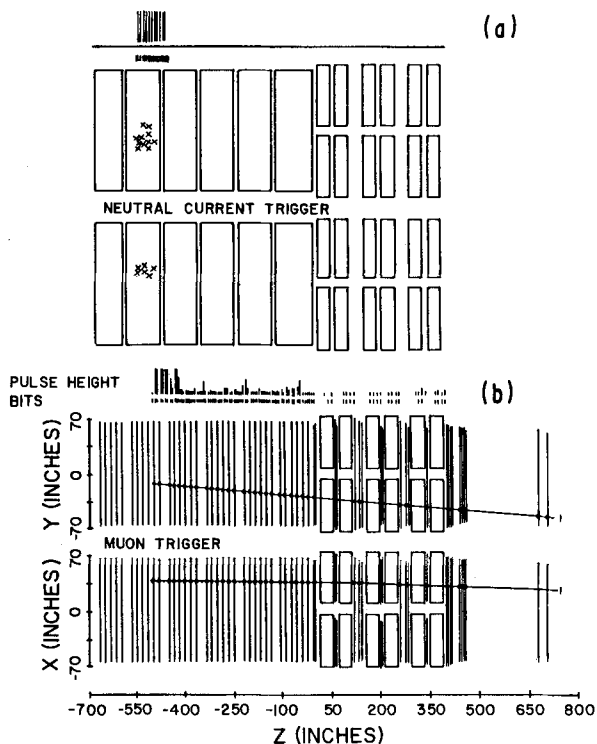


Fig. 3a, b. The Lab-E neutrino detector used for both E616 and E701: a shows a typical NC event; b shows a CC event, with the muon appearing in counter pulse heights and in chamber hits

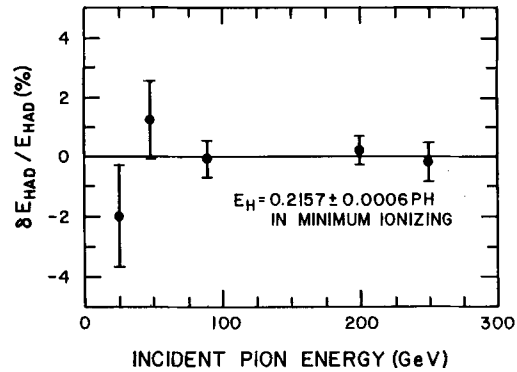


Fig. 4. Deviations of best fit from measured hadron energy calibration as a function of hadron beam energy

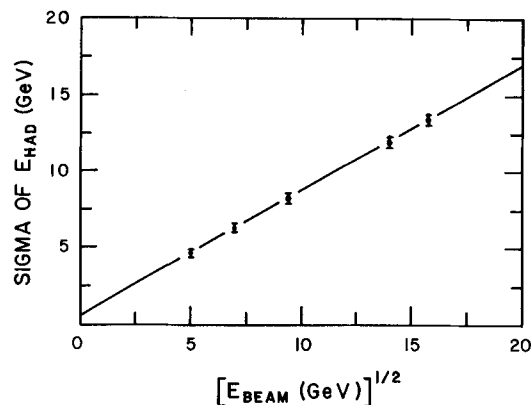


Fig. 5. Sigma of measured hadron energy as a function of beam energy

The calorimeter counters were used to measure the hadron energy of events, as well as the longitudinal vertex and the range of penetration of charged particles. They have been extensively mapped using beam muons and hadron showers from a momentum-defined test beam, and these map corrections were applied in determining hadron energy in neutrino interactions. The calibration and resolution of the calorimeter have been measured [5] in test runs with hadron beams both before and after the data presented here were recorded. The linearity of the calibration is shown in Fig. 4. With hadron beam energies of 25, 50, 90, 200, and 250 GeV, the resolution was found to be fitted well by the expression

$$\delta E_{had}(\text{GeV}) = (0.72 \pm 0.20) + (0.81 \pm 0.03) \sqrt{E_{had}(\text{GeV})} \quad (3)$$

as shown in Fig. 5.

Event reconstruction

From (1) and (2), R^ν is insensitive to $\sin^2\theta_W$ (for $\rho = 1$ and $\sin^2\theta_W \approx 0.24$), so the measurement of R^ν has little effect on the determination of $\sin^2\theta_W$. The important

ratio is R^{ν} ; an error of $\pm 1\%$ in R^{ν} produces an error of ∓ 0.005 in $\sin^2\theta_w$. Since a precise measurement of R^{ν} was required in this experiment, it was imperative to minimize any possible bias between NC and CC events, both in event selection and event analysis.

Consequently, even though the production angle and energy of the final state lepton were measured for most CC events, this information was not directly used in the neutral current analysis. Only information that was measured equally well for both NC and CC events contributed directly to the analysis. This requirement was a major factor in determining the analysis procedure, e.g. the event trigger, the vertex finding algorithm, and the cuts imposed on the interaction point and hadron energy.

The trigger electronics contained several independent triggers, including a “muon trigger” (requiring a penetrating charged particle) and a “hadron trigger” (requiring only a localized energy deposition in the calorimeter). To avoid any bias between CC and NC events, only events satisfying the “hadron trigger” were used in the determination of R^{ν} . This trigger required 2 counters in a group of 4 adjacent calorimeter counters to fire in coincidence with ≥ 10 –15 GeV of energy deposition measured in these 4 counters plus the 8 counters immediately downstream. E701 was run with lower counter thresholds to give better efficiency at low E_{had} . In both experiments, the efficiency of the hadron trigger was monitored by comparison with the muon trigger used for CC events. This efficiency is shown as a function of hadron energy E_{had} in Fig. 6 for both experiments E616 and E701. In the analysis of each experiment, a software cut of $E_{\text{had}} \geq 20$ GeV was imposed to ensure that the trigger was 100% efficient for both NC and CC events.

The only reconstructed quantities used in the analysis were those which we believe were measured equally well for both NC and CC events: these are

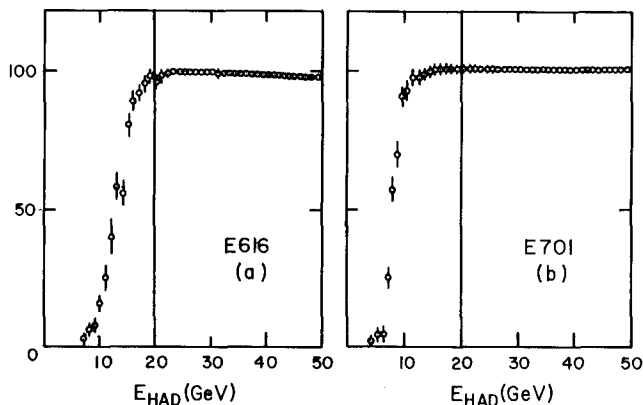


Fig. 6a, b. Neutral current trigger efficiencies for both experiments as a function of measured E_{had}

the longitudinal and transverse coordinates of the interaction point, the total hadron energy, and the “event length”, defined as the maximum penetration distance of charged particles produced by the interaction.

The longitudinal (z) vertex position along the beam axis was found from the group of counters showing energy deposition around the interaction point, and was defined to be the center of the steel plate immediately upstream of the most upstream counter in this group. Spark chamber information was not used.

The transverse vertex of the event was found from a weighted average of the hits in the 6 spark chambers immediately downstream of the vertex (i.e., in the hadron shower). Charged-current muon track information was not used, in order to avoid bias between NC and CC events. The transverse vertex was checked for a sample of CC events by comparing it to the vertex obtained by extrapolating the muon track to the z -coordinate of the interaction vertex. The *rms* difference of the two definitions was ≈ 4.3 cm in both the x and y coordinates.

The hadron energy E_{had} of an event was obtained by summing the calibrated ionization measured in the 21 calorimeter counters immediately downstream of the event vertex. As described above, the calibration of each counter was monitored by measuring the muon ionization peak throughout the run. Map corrections, measured as a function of transverse position, were applied to the pulse-height of each counter, and the calibration ratio used to convert total ionization into hadron energy was measured in test runs using hadron beams. For CC events, it was necessary to subtract the ionization due to the penetrating muons. This subtraction was measured separately for each beam setting, using unambiguously identified CC events, by summing groups of 21 counters in regions well downstream of the hadron shower.

The event length L was defined to be the distance (in meters of steel) between the most upstream and the most downstream of the contiguous calorimeter counters showing ionization. The event length was therefore the range of the most penetrating charged particle produced at the event vertex. For NC events, this was the range of the hadron shower; for CC events, it was the typically much longer range of the penetrating muon. The event length was the single measured parameter used to separate NC and CC events, as described below.

Event classifications

In order to utilize the band structure of the neutrino beam, the measured E_{ν} spectrum of fully reconstructed CC events was used to determine, for each beam

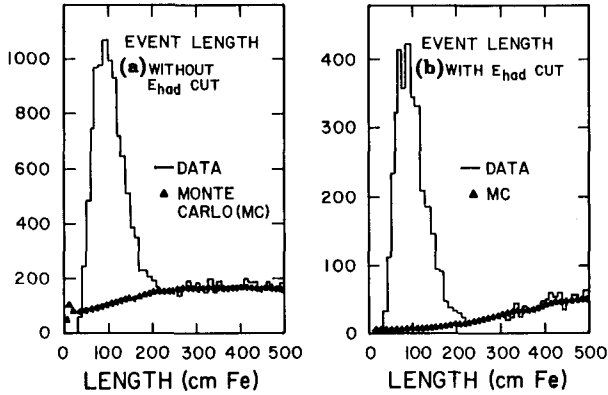


Fig. 7a, b. Event length L for all events: **a** without the $E_{\text{had}}(r)$ cut, and **b** with the $E_{\text{had}}(r)$ cut which removes most of the CC background at low L . Note that the Monte-Carlo calculation of L uses only the muon length

setting, a separation curve $E_s(r)$ lying in the valley between the π and K bands in the E_ν vs. r plane (see Fig. 2). Since only E_{had} (not E_ν) could be used in the neutral current analysis, all interactions were classified as “ π -band” if $E_{\text{had}} < E_s(r)$, and as “ K -band” if $E_{\text{had}} > E_s(r)$. This left a background of ν_K events with low E_{had} in the π band, but since the ν_π events were far more numerous, the background was small and calculable. This procedure made it possible to measure $R^{\nu, \bar{\nu}}$ for each band and each beam setting.

NC and CC events were distinguished in each band on the basis of length. If all events at a given beam setting are histogrammed as a function of length, the neutral currents appear as a peak in the short-length region ($L \leq 2.1$ m Fe), while the CC events form a plateau extending up to very long length (see Fig. 7). However, several corrections must be made to these two regions in order to extract accurate NC and CC signals.

Measured corrections to NC and CC classes

Interactions due to cosmic rays entering through the top or sides of the detector frequently gave short-length showers, and tended to mimic neutral current interactions. This background was minimized by using the fast spill extraction described earlier. The remaining background was directly measured by taking data in a 10-ms “cosmic ray” gate after each beam cycle throughout the run. The live-time of the detector was recorded for each beam gate and for each cosmic ray gate. In the analysis, cosmic ray events taken during running at a given secondary beam setting were treated in exactly the same way as neutrino events taken at that beam setting. After all cuts, the cosmic ray rates for each class were subtracted from the beam rates, using the integrated livetimes for relative normalization. Although the subtraction applied to the

short-length class was significant (2.1%), the errors were quite small ($\pm 0.1\%$).

Pions and kaons which decayed upstream of the momentum-selecting collimator produced a small background of “wide-band” neutrinos, which tended to be low-energy and uniformly spread over the detector. Since it was impossible to reliably calculate the spectrum of these neutrinos, their contamination was measured by running the experiment at each beam setting with the momentum-selecting collimator closed. After correcting these wide-band rates for cosmic ray backgrounds, they were subtracted from the beam rates at each beam setting, normalized to the integrated proton flux. The total subtraction to the short-length region was $(1.7 \pm 0.4)\%$ summed over all beam settings. Since wide-band events contributed to both the NC and CC regions, the effect of the subtraction on R^ν was much smaller.

Large hadron showers had a small but non-negligible probability of extending beyond the 21-counter length cut; this “punch-through effect” tended to shift events from the NC class to the CC class. The probability of punch-through was measured as a function of E_{had} by running a monoenergetic hadron beam into the neutrino detector, at energies of 25, 50, 90, and 200 GeV. The probability P that a hadron shower extended beyond the 2.1 m cut was well fitted throughout this energy range by a linear parameterization: $P(L \geq 2.1 \text{ m Fe}) = 1.15 \times 10^{-4} E_{\text{had}}$. At each beam setting, this formula was integrated over the measured short-length E_{had} spectrum to obtain the punch-through component, which was then subtracted from the NC class and added to the CC class; this correction amounted to $0.7 \pm 0.1\%$ of the total short-length event sample.

Corrections for each of these measured backgrounds were made separately to the short- and long-length regions in each energy band and for each beam setting. The cosmic ray and wide-band backgrounds were further reduced by cuts in E_{had} described below. The net uncertainty in R^ν due to these measured corrections was 0.3%, mainly due to statistical error in the wide-band background subtraction. This produced a small uncertainty in $\sin^2 \theta_W$ of ± 0.0015 , which is included in the statistical error.

Monte-Carlo simulation of beam and detector

Several other backgrounds and correction factors could not be directly measured, and were calculated using a detailed Monte-Carlo simulation of the beam and the detector. In the Monte Carlo simulation, secondary particle rays were traced through the dichromatic train and decayed through the reactions $\pi \rightarrow \mu \nu_\mu$, $K \rightarrow \mu \nu_\mu$, $K \rightarrow \pi^0 \mu \nu_\mu$, $K \rightarrow \pi^0 e \nu_e$, with branching ratios of 100%, 63.5%, 3.2%, and 4.9% respec-

tively. Events were generated in the detector using structure functions previously obtained [5] in a fit to the E616 CC data. The event generation included the effects of radiative corrections using the method described in [6].

For each beam setting, the centroids of the distributions in transverse vertex of the Monte-Carlo events were adjusted to agree with the measured centroids of data events. Their interaction z coordinates were generated according to the distribution of matter in the calorimeter. The fiducial cuts used in the data analysis were then applied.

All generated hadron showers were given a range of less than 2.1 m of steel, since the data had already been corrected for “punch-through” showers. The event length for generated CC events was determined solely by the muon, and was equal to the length in steel between the event vertex and the point where the muon either ranged out or left through the sides of the calorimeter. As in the data analysis, Monte-Carlo events with length ≤ 2.1 m of steel were classified as “short-length” events, and events with length ≥ 2.1 m were classified as “long-length”.

For all Monte Carlo events, the generated hadron energy was smeared by the detector resolution. To simulate the definition of E_{had} for data events, Monte Carlo CC events had the ionization energy loss of the muon in the 2.1 m of steel downstream of the interaction point added to the smeared hadron energy. This ionization energy loss was dependent on muon momentum, and was obtained from momentum-binned data distributions of muon energy loss in CC events. In analyzing the Monte Carlo events in the long-length class, the data analysis was copied by subtracting an average muon ionization energy loss in 2.1 m of steel for each beam setting. An average (instead of momentum dependent) subtraction was used since not all data charged-current muons passed through the good-field region of the muon spectrometer (required for good momentum measurement). The E_{had} obtained by this procedure was used for the 20 GeV E_{had} cut, and to separate MC events into ν_π and ν_K classes, in the same way as for data.

Calculated corrections to NC and CC classes

The data included background events from neutrinos produced by the three-body decays of kaons, $K \rightarrow \mu \nu_\mu \pi^0$ and $K \rightarrow e \nu_e \pi^0$. These neutrinos did not have the energy-radius correlation characteristic of the dichromatic beam; in addition, electron neutrinos produced short ranged electromagnetic showers which contaminated only the short-length class and therefore had a significant effect on R^ν . Both of these backgrounds were subtracted using the Monte-Carlo,

normalized to reproduce the correct numbers of events in the long-length kaon bands.

As discussed earlier, the ν_π class had a background of ν_K events with low E_{had} . Due to the momentum spread of the beam, there was also a very small background of ν_π events in the ν_K class. These backgrounds were subtracted, and R^ν values were formed separately for the ν_π and ν_K classes.

A more serious background came from CC events with very low-energy muons which either ranged out or left the sides of the calorimeter with $L \leq 2.1$ m. These were extrapolated from the long-length CC distribution using the Monte Carlo, and both the short- and long-length regions were corrected for this effect. In order to minimize the dependence of this extrapolation on the assumed CC structure functions, the Monte-Carlo subtraction was normalized to the number of CC events which had $L > 2.1$ m Fe and which also either ranged out or left through the sides of the calorimeter rather than through the downstream end. In this way, only the medium-length CC events, which were kinematically most similar to the short-length background events, were used to normalize the subtraction.

If no further cuts had been applied to the data, this would have been the largest background and the largest source of experimental systematic error in the analysis. However, the use of the narrow-band neutrino beam made it possible to remove most of these ambiguous events by means of a cut on measured hadron energy. Both classes of short-length CC events, with muons which escaped or which ranged out, necessarily had low-energy muons and therefore high-energy hadron showers. Since the maximum muon production angle increases with increasing E_{had} , almost all of this background could be eliminated by rejecting all events, both NC and CC, which had $E_{\text{had}} > E_{\text{had}}^{\text{cut}}(r)$. $E_{\text{had}}^{\text{cut}}(r)$ was defined so that an event with the expected energy $E_\nu(r)$ at radius r and with $E_{\text{had}} > E_{\text{had}}^{\text{cut}}(r)$ would necessarily have $L > 2.1$ m of Fe.

The cut in E_{had} corresponded roughly to a cut in $y(=E_{\text{had}}/E_\nu(r)) \geq 0.7$, but the exact effect of the cut depended on beam setting and radius r of the event vertex. The data sample was reduced by about a factor of 2 by this cut, but the background was reduced by a factor of 10 (see Fig. 7b). The remaining CC background in the short-length region was due to the finite momentum spread and dispersion of the secondary beam, and to the finite resolution in measured E_{had} and vertex position, and this was calculated using the Monte Carlo. Because $E_{\text{had}}^{\text{cut}}(r)$ became smaller with increasing r , this cut was most severe at larger r . It consequently removed more events near the edges of the detector, and had the effect of reducing the relative cosmic ray background from 2.1%

Table 1. Corrections made to the short-length region ($L \leq 21$ counters), expressed as a fraction of the final NC data sample. The radius-dependent E_{had} cut has been applied

Measured corrections		Calculated backgrounds	
Cosmic rays: (from 10-ms CR gate)	-1.2%	ν_{μ} from $K_{\mu 3}$ decays:	-0.9%
		ν_e from $K_{e 3}$ decays:	-8.1%
Wide band background: (measured with slit closed)	-0.8%	ν_{π} in K-band:	-0.9%
		ν_{κ} in π -band:	-10.8%
Hadronic punch-thru: (from test beam data)	+0.8%	CC interactions with $L \leq 21$	-6.1%

Table 2. R_{meas}^{ν} from E616 and E701

Experiment	particle	E_{had}	no $E_{\text{had}}(r)$ cut	with $E_{\text{had}}(r)$ cut
E616	pion	250	0.287 ± 0.015	0.303 ± 0.016
		200	0.291 ± 0.013	0.285 ± 0.014
		165	0.299 ± 0.015	0.286 ± 0.018
		140	0.286 ± 0.018	0.308 ± 0.023
		120	0.304 ± 0.023	0.278 ± 0.030
E616	kaon	250	0.283 ± 0.019	0.275 ± 0.022
		200	0.319 ± 0.021	0.321 ± 0.026
		165	0.320 ± 0.027	0.269 ± 0.034
		140	0.258 ± 0.034	0.263 ± 0.051
		120	0.393 ± 0.057	0.397 ± 0.099
E701	pion	250	0.287 ± 0.014	0.293 ± 0.013
		200	0.289 ± 0.012	0.303 ± 0.012
		165	0.275 ± 0.018	0.326 ± 0.020
		140	0.302 ± 0.012	0.316 ± 0.015
		100	0.266 ± 0.020	0.244 ± 0.032
E701	kaon	250	0.292 ± 0.020	0.299 ± 0.025
		200	0.279 ± 0.023	0.264 ± 0.031
		165	0.294 ± 0.036	0.320 ± 0.058
		140	0.317 ± 0.028	0.283 ± 0.046
		100	0.263 ± 0.048	0.255 ± 0.137

to 1.2%, and the wide-band background from 1.7% to 0.8%.

All of these corrections were made to both energy bands at each beam setting. The sizes of all of these corrections to the short-length region, both measured and calculated, are summarized in Table 1. After all corrections, the NC to CC ratios were calculated for each band and each beam setting by dividing the number of corrected short-length events by the corrected number of long-length events. These measured values, which will be referred to as R_{meas}^{ν} and $R_{\text{meas}}^{\bar{\nu}}$, are given in Table 2 and 3, and plotted in Figs. 8 and 9. A weighted average of all the R_{ν} values gave:

$$R_{\nu} = 0.291 \pm 0.006 \quad \text{with } E_{\text{had}} \leq E_{\text{had}}^{\text{cut}}(r) \quad (4)$$

and

$$R_{\nu} = 0.299 \pm 0.005 \quad \text{with no high-} E_{\text{had}} \text{ cut.} \quad (5)$$

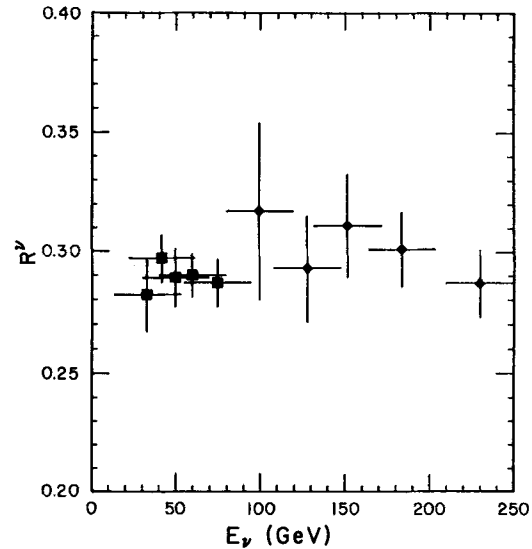


Fig. 8. R_{ν}^{ν} , from E616 and E701 combined, as a function of E_{ν} . These are the ratios before the $E_{\text{had}}(r)$ cut is applied

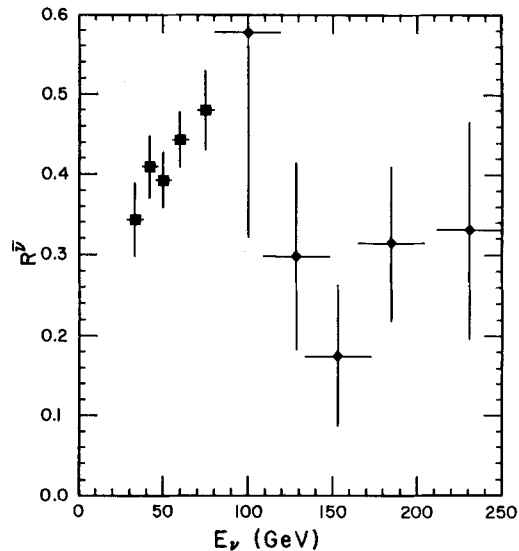


Fig. 9. R_{ν}^{ν} , from E616, plotted as a function of E_{ν} . These are the ratios before the $E_{\text{had}}(r)$ cut is applied

Table 3. R_{meas}^{ν} from E616 (used only in 2-parameter fit)

particle	E_{beam}	no $E_{\text{had}}(r)$ cut	with $E_{\text{had}}(r)$ cut
pion	250	0.480 ± 0.050	0.466 ± 0.047
	200	0.443 ± 0.035	0.396 ± 0.034
	165	0.392 ± 0.035	0.388 ± 0.040
	140	0.409 ± 0.039	0.374 ± 0.046
	120	0.343 ± 0.046	0.299 ± 0.061
kaon	250	0.331 ± 0.135	0.375 ± 0.175
	200	0.314 ± 0.096	0.473 ± 0.132
	165	0.174 ± 0.088	0.166 ± 0.110
	140	0.298 ± 0.116	0.208 ± 0.126
	120	0.578 ± 0.257	0.427 ± 0.315

Extraction of $\sin^2 \theta_W$ and ρ

The measured values R_{meas}^{ν} and $R_{\text{meas}}^{\bar{\nu}}$ incorporate all the corrections discussed earlier, including corrections for cosmic ray and wide band backgrounds, subtraction of short length CC events from the NC class, removal of $Ke3$ and $K\mu3$ backgrounds, and removal of the background of ν_K events with low E_{had} which contaminate the ν_{π} class.

The electroweak parameters ρ and $\sin^2 \theta_W$ can be extracted from R_{meas}^{ν} and $R_{\text{meas}}^{\bar{\nu}}$ through the use of the theoretical relationships of (1) and (2):

$$R_{\text{theor}}^{\nu} = \rho^2 \left(\frac{1}{2} - \sin^2 \theta_W + \frac{5}{9} \sin^4 \theta_W (1+r) \right)$$

and

$$R_{\text{theor}}^{\bar{\nu}} = \rho^2 \left(\frac{1}{2} - \sin^2 \theta_W + \frac{5}{9} \sin^4 \theta_W \left(1 + \frac{1}{r} \right) \right).$$

However, these equations were derived from an idealized model. R_{meas}^{ν} and $R_{\text{meas}}^{\bar{\nu}}$ are shifted from the ideal theoretical values R_{theor}^{ν} and $R_{\text{theor}}^{\bar{\nu}}$ by various effects which include the finite width of the neutrino beam energy spectrum, E_{had} smearing due to detector resolution, the non-isoscalar target, the finite strange quark sea [7], charm production with slow rescaling [8], and radiative corrections [6] to the charged-current differential cross-section. It was therefore neces-

sary to correct R_{meas}^{ν} and $R_{\text{meas}}^{\bar{\nu}}$ before using (1) and (2).

These corrections were made by applying multiplicative correction factors, f^{ν} and $f^{\bar{\nu}}$, to R_{meas}^{ν} and $R_{\text{meas}}^{\bar{\nu}}$. To obtain these correction factors, simulated values R_{sim}^{ν} and $R_{\text{sim}}^{\bar{\nu}}$ were obtained by a Monte Carlo simulation of the measurement for each beam setting. The simulation included the various effects described above as well as electromagnetic radiative corrections from virtual photon diagrams and bremsstrahlung by the final state charged current muon. Monte Carlo events were subjected to the same cuts and analysis procedures as data events.

The Monte Carlo simulation used input values $\sin^2 \theta_{W_0} = 0.225$ and $\rho_0 = 1$, which were substituted into (1) and (2) to give $R_{\text{theor}}^{\nu}(\sin^2 \theta_{W_0})$, corresponding to an idealized beam, target, and detector. The values of $r = \sigma_{\text{CC}}^{\bar{\nu}} / \sigma_{\text{CC}}^{\nu}$ in the theoretical expressions came from the Monte Carlo simulation, using the measured [5] CC structure functions. The correction factors were defined to be $f^{\nu} \equiv R_{\text{theor}}^{\nu}(\sin^2 \theta_{W_0}) / R_{\text{sim}}^{\nu}(\sin^2 \theta_{W_0})$. They were found for each beam setting, for the ν_{π} and ν_K classes, with and without the radius dependent E_{had} cut. The absolute deviation of f^{ν} from unity was $\leq 1\%$ for the ν_{π} class, and was $\approx 4\%$ on average for the ν_K class (ν_K events have higher energies than ν_{π} events, and are more likely to produce heavy charmed quarks). The individual corrections that enter into f^{ν} and their associated errors are described in the following section.

In addition to the correction factors entering into f^{ν} , a theoretical electroweak correction had to be made which depended on the exact definition of $\sin^2 \theta_W$ and on the renormalization scheme adopted. The ratio $R^{\nu} = \sigma_{\text{NC}}^{\nu} / \sigma_{\text{CC}}^{\nu}$ can be schematically represented in terms of Feynman diagrams as shown in Fig. 10. In both numerator and denominator, the first (Born) term arises from the exchange of a gauge boson. The second term is due to a gauge boson self-energy diagram which cancels in the calculation of R^{ν} . There are three additional diagrams in the denominator which do not appear in the numerator, and therefore give the ratio a slight Q^2 dependence. Two of these are QED diagrams which were incorporated

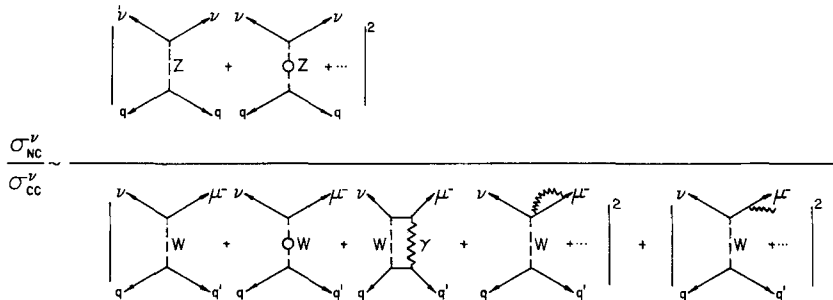


Fig. 10. $R^{\nu} = \sigma_{\text{NC}}^{\nu} / \sigma_{\text{CC}}^{\nu}$ represented in terms of Feynman diagrams, showing the electroweak correction terms which apply to both numerator and denominator

in the Monte Carlo. The third is a $W\gamma$ box diagram. The electroweak radiative correction due to this diagram depends on the renormalization scheme used. We have chosen the convention in which $\sin^2\theta_W$ is defined by

$$\sin^2\theta_W \equiv 1 - M_W^2/M_Z^2 \quad (6)$$

where M_W and M_Z are the physical gauge boson masses. When this convention is used, the theoretical value of R^ν is reduced in the low Q^2 range of this experiment ($Q^2 \leq 500$ GeV) by a factor $f_{W\gamma} = 0.983$. In theoretical calculations [9] of this factor, no y cuts have been applied; however, the dependence of $f_{W\gamma}$ on Q^2 and y is negligible over the entire kinematic range of the experiment and so $f_{W\gamma}$ can be factored out as a constant multiplicative scale factor. Two further higher order radiative corrections to $\sin^2\theta_W$ were not included because they almost exactly cancel: -0.0007 from terms containing logarithms of quark masses, and $+0.0007$ from vertex diagrams involving photons and γZ mixing diagrams.

We therefore expect R_{meas}^ν and R_{theor}^ν , for each beam setting, to be related by

$$f_i^\nu R_{\text{meas}i}^\nu = f_{W\gamma} R_{\text{theor}i}^\nu \quad (7)$$

where $R_{\text{theor}i}^\nu \equiv \rho^2 (\frac{1}{2} - \sin^2\theta_W + \frac{5}{9} \sin^4\theta_W (1+r_i))$. A χ^2 of the form

$$\chi^2 = \frac{\sum_i (f_i^\nu R_{\text{meas}i}^\nu - f_{W\gamma} R_{\text{theor}i}^\nu)^2}{\sigma_{R_i^\nu}^2} \quad (8)$$

was minimized with $\sin^2\theta_W$ as the only free parameter: ρ was fixed at the value $\rho=1$ predicted by the Weinberg-Salam model for the simplest choice in the Higgs sector. The index i in (7) and (8) ran over the ν_K and ν_π classes for the different beam settings.

The fitted values of $\sin^2\theta_W$ resulting from this procedure are summarized in Table 4. The χ^2 values for E616 and E701 were obtained from a global χ^2 minimization using the data from both experiments. The errors quoted in Table 4 are statistical only; the systematic errors are discussed later. The small difference between the value for E616 quoted here and that of [1] is due primarily to a small improvement in the algorithm used to find E_{had} .

Table 4. $\sin^2\theta_W$ from 1-parameter fits ($\rho \equiv 1$) (statistical error only)

	no $E_{\text{had}}(r)$ cut	with $E_{\text{had}}(r)$ cut
E616	0.234 ± 0.009	0.243 ± 0.011
E701	0.242 ± 0.009	0.236 ± 0.010
E616 + E701	0.238 ± 0.006	0.239 ± 0.008

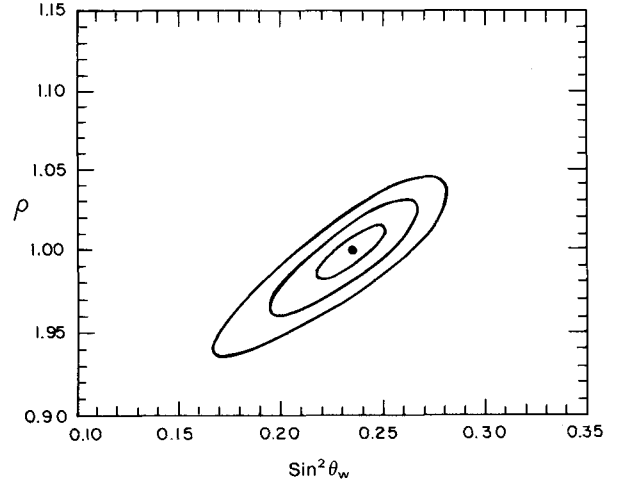


Fig. 11. The 1, 2, and 3 sigma contours resulting from a 2-parameter fit to R^ν and $R^{\bar{\nu}}$. No $E_{\text{had}}(r)$ cut is applied, since statistical error dominates

As mentioned earlier, $\sin^2\theta_W$ can be extracted from R^ν only since the value of $\sin^2\theta_W$ is totally insensitive to $R^{\bar{\nu}}$. To measure ρ , however, it was necessary to use a χ^2 containing both R^ν and $R^{\bar{\nu}}$. This χ^2 was then minimized allowing both ρ and $\sin^2\theta_W$ to be free parameters. This was done for the E616 data sample, where there was antineutrino running at each beam setting. Without the radius-dependent E_{had} cut, we obtained

$$\rho = 1.000 \pm 0.018, \quad \text{and} \quad \sin^2\theta_W = 0.234 \pm 0.018. \quad (9)$$

With the radius-dependent E_{had} cut, we obtained

$$\rho = 1.005 \pm 0.023, \quad \text{and} \quad \sin^2\theta_W = 0.248 \pm 0.025. \quad (10)$$

The errors quoted above are statistical only; the systematic error in ρ is discussed later. The 1, 2 and 3 σ contours for the two parameter fit are shown in Fig. 11 (with radius dependent E_{had} cut).

Physical effects determining the correction factors f^ν

As described above, the f^ν correction factors used to extract $\sin^2\theta_W$ incorporated all the physical effects (e.g. the non-isoscalar target and charm production) which deviate from the idealized model in which (1) and (2) are strictly true. The sensitivity of the extracted $\sin^2\theta_W$ value to each of these effects was investigated by recalculating the f^ν correction factors under different sets of physical assumptions. When $\sin^2\theta_W$ was extracted using the recalculated f^ν values, the r_i values in (7) and (8) were held fixed at the values used in the standard analysis. The background subtractions from the data sample were also those used in the standard analysis.

The f^ν values for the ν_K and ν_π classes were first obtained by generating Monte Carlo events assuming an isoscalar target with no strange sea quarks and with zero charm quark mass (this is the ideal case in which (1) is strictly true). However, these f^ν values were not identically equal to unity because the Monte Carlo simulation included the effects of the neutrino beam energy spectrum and hadron energy smearing due to detector resolution. In the analysis of Monte Carlo events, the ionization energy loss of short length charged-current events was added to the hadron energy, in order to simulate the analysis of data events. This was particularly important in simulating the effect of the radius dependent E_{had} cut on the data sample.

Each Monte Carlo NC or CC event was then reweighted for each new set of physical assumptions. This was done by fixing the transverse and longitudinal position of the interaction vertex, the incident neutrino energy E_ν , and the values of the kinematic x and y variables ($x = Q^2/2ME_{\text{had}}$, $y = E_{\text{had}}/E_\nu$). The recalculated weight of the event was the ratio of the differential cross-section under the new set of physical assumptions to the differential cross-section under the original set of assumptions. For each set of physical assumptions, the f^ν values for the ν_π and ν_K classes at the different beam settings were recalculated from the reweighted Monte Carlo events. These f^ν values were then used to extract a value of $\sin^2\theta_W$. The effects of the different physical assumptions on $\sin^2\theta_W$ are listed in Table 5. The physical assumptions were changed in the following order:

First, the strange and antistrange quarks were introduced. This changed the composition of the $q\bar{q}$ sea while leaving the overall level of the sea fixed. The largest effect was to change some u and d sea quarks into s ; this increased the number of CC events (since an incident ν can interact only with d and s , and not with u) and hence decreased R_{sim}^ν . The decrease in R_{sim}^ν shifted f^ν upward, and hence decreased $\sin^2\theta_W$ as shown in Table 5.

Next, the mass of the charm quark was increased to 1.5 GeV. This decreased the CC cross-section due

Table 5. Corrections to $\sin^2\theta_W$ incorporated in f^ν

	no E_{had} cut	with E_{had} cut
s, \bar{s} quarks	-0.011	-0.010
$m_c = 1.5 \text{ GeV}/c^2$	+0.014	+0.015
non-isoscalar target	-0.009	-0.009
electromagnetic rad. corr.	-0.004	-0.002
electroweak rad. corr.	-0.009	-0.009
Total	-0.019	-0.015

to threshold and slow-rescaling effects, and therefore increased $\sin^2\theta_W$. This cancelled much of the decrease in R^ν caused by introducing the strange quarks, since interactions with the strange sea predominantly produce charm. Since d quarks also produce charm (with a factor of $\sin^2\theta_C$), the total suppression of CC production more than cancelled the effect of introducing strange quarks.

Next the isoscalar correction was introduced. This turned some u quarks into d quarks, increasing the number of CC events and hence decreasing $\sin^2\theta_W$.

Finally, electromagnetic radiative corrections were introduced. Since muon bremsstrahlung increased the apparent E_{had} , this caused more CC events to pass the $E_{\text{had}} > 20 \text{ GeV}$ cut and therefore decreased R^ν .

The total correction from all of these effects decreased the value of $\sin^2\theta_W$ obtained by 0.015 with the $E_{\text{had}}(r)$ cut, and by 0.019 without. It is interesting that most of the change is due to corrections to the CC cross-section, rather than to the NC cross-section.

Systematic errors

Systematic errors can be divided into (1) experimental systematic errors inherent in the measurement and analysis procedures used in this experiment, and (2) theoretical systematic errors common to all measurements of $\sin^2\theta_W$ from deep-inelastic neutrino-nucleon

Table 6. Systematic errors in $\sin^2\theta_W$ (1-parameter fit)

	no $E_{\text{had}}(r)$ cut	with $E_{\text{had}}(r)$ cut
Experimental errors:		
uncertainty in CC subtraction:		
– due to quark x distributions	± 0.010	± 0.002
– due to M.C. beam dispersion	± 0.001	± 0.003
Mean π, K momentum	± 0.002	± 0.002
Secondary beam momentum bite	± 0.001	± 0.002
Hadron energy ($\delta E_{\text{had}} < \pm 2\%$)	± 0.003	± 0.002
Miscellaneous	± 0.002	± 0.003
Total	± 0.011	± 0.006
Theoretical errors:		
uncertainty in overall level of $q\bar{q}$ sea and strange quark content ($s/\bar{u} = 0.5 \pm 0.2$)	± 0.002	± 0.002
$\cos\theta_{\text{cabibbo}} = 0.9737 \pm 0.0025$	± 0.002	± 0.002
Radiative corrections	± 0.003	± 0.002
$m_c = 1.5 \pm 0.4 \text{ GeV}/c^2$	± 0.006	± 0.006
Total	± 0.007	± 0.007

scattering in the Q^2 range of this experiment. The experimental and theoretical systematic errors in this measurement of $\sin^2\theta_W$ are given in Table 6.

Experimental systematic errors in $\sin^2\theta_W$

The uncertainty in the CC background subtraction from the NC sample is largely due to uncertainty in the shapes of the quark x distributions used in the Monte Carlo. This uncertainty in the subtraction is proportional to the size of the subtraction. This motivated the use of the radius dependent E_{had} cut, which greatly reduced the size of the CC subtraction.

The uncertainty in this subtraction was estimated by varying structure function parameters within their statistical errors and noting the resulting change in the subtraction. The tabulated uncertainty also includes the slight differences in the subtraction when different methods are used to normalize Monte Carlo to data. Another minor source of uncertainty in the subtraction is the occasional backscatter of nuclear fragments in the hadron shower, which may lead to a small shift in the location of the interaction vertex.

The effect of the above uncertainties leads to a combined uncertainty of 3.5% in the CC subtraction without the radius dependent E_{had} cut, i.e. an uncertainty of ± 0.010 in $\sin^2\theta_W$. When the radius dependent E_{had} cut is applied, the CC subtraction, and therefore the uncertainty in $\sin^2\theta_W$, is reduced by a factor of 5.

A final source of uncertainty in the charged-current subtraction is due to the fact that the angular dispersion of Monte Carlo secondary particles may not exactly match that of the actual beam. This was studied by changing the angular dispersion produced by the Turtle [10] program used to simulate the narrow-band train. It was found that the value of $\sin^2\theta_W$ without the radius dependent E_{had} cut was insensitive to the angular dispersion; the error in $\sin^2\theta_W$ with the cut was estimated to be < 0.002 .

Uncertainties in the mean secondary particle momentum and the secondary particle momentum bite could lead to a mismatch between the Monte Carlo beam and the actual beam. The mean secondary momentum was taken to be uncertain by $\pm 1.5\%$ and the momentum bite was taken to be $9\% \pm 1\%$.

The uncertainty in the measured E_{had} was conservatively estimated to be $\pm 2\%$, due to the uncertainty in the calibration and the correction to the pulse height as a function of position in the scintillation counters.

Finally, Table 6 lists a miscellaneous experimental systematic error which includes the Monte Carlo sta-

tistical error in calculating the f^ν correction factors, and the effect of variations in the details of the fitting procedure.

Theoretical systematic errors in $\sin^2\theta_W$

The size of the quark-antiquark sea was taken to be uncertain by $\pm 10\%$; in addition, s/\bar{u} , the strange quark fraction of the sea, was taken to be 0.5 ± 0.2 . These uncertainties introduced an error of ± 0.002 in $\sin^2\theta_W$. Uncertainties in the simulation of charm production arose from uncertainties in the Cabibbo angle ($\cos\theta_C = 0.9737 \pm 0.0025$) and the mass m_C of the final state charm quark. The largest and most uncertain of the theoretical corrections is the one for the charmed quark mass. Some authors [11] have used an effective mass as low as 1.1 GeV, or one that depends on Q^2 ; an upper limit on the effective mass is given by the D mass of 1.9 GeV. But the whole slow-rescaling picture may not be correct in detail. We have assumed a fixed mass of 1.5 GeV with a large error of ± 0.4 GeV to take these uncertainties into account. This is our dominant theoretical error. The value of $\sin^2\theta_W$ extracted was found to increase linearly with the value of m_C^2 used, in the range $m_C = 1.1$ to 1.9 GeV/ c^2 . The extracted value of $\sin^2\theta_W$ was reduced by 0.005 when m_C was reduced from 1.5 to 1.1 GeV/ c^2 .

The uncertainty in our radiative correction is estimated [12] to result in a systematic error in $\sin^2\theta_W$ of $\leq 1\%$. This analysis uses a simple radiative correction procedure which contains all the relevant physical processes. Independent calculations by other neutrino collaborations result in total radiative corrections to $\sin^2\theta_W$ which differ from the correction in this analysis by $\leq \pm 0.003$ without the radius dependent E_{had} cut. This agrees well with the 1% uncertainty mentioned above. As discussed earlier, the size (and uncertainty) of the electromagnetic radiative correction is larger without the radius dependent E_{had} cut.

Each of these corrections should be very similar for all deep-inelastic scattering experiments, although there will be differences due to different target materials, beam spectra, and cuts in E_{had} .

In correcting for the strange sea, we have assumed [7] that strange quarks have the same x distribution as \bar{d} -quarks, but that $s/\bar{d} = 0.5$, i.e., the sea is half SU3 symmetric. In simulating charmed quark production, we have assumed a fixed quark mass of 1.5 GeV and have used the slow-rescaling formalism [8]. For the non-isoscalar correction, we have used a calculated neutron excess of $(n-p)/(n+p) = 0.071$ for our target (mainly Fe).

Systematic errors in ρ

The normalization factor ρ , defined by (1) and (2), is determined by simultaneously fitting R^ν and $R^{\bar{\nu}}$. Since E701 recorded a very small amount of antineutrino data, we have used only the E616 measurements of both R^ν and $R^{\bar{\nu}}$ in determining ρ . Since $R^{\bar{\nu}}$ is insensitive to $\sin^2\theta_W$, ρ is determined primarily by the measurement of R^ν . The systematic error in R^ν (about 2%) is somewhat larger than that in $R^{\bar{\nu}}$, primarily due to the uncertainty in m_C .

However, ρ is less sensitive than $\sin^2\theta_W$ to errors in R^ν and $R^{\bar{\nu}}$. From (1), an error of 1% in R^ν produces an error of about 2% in $\sin^2\theta_W$; but from (2), an error of 1% in $R^{\bar{\nu}}$ produces an error in ρ of only 0.5%. Moreover, the statistical errors in $R^{\bar{\nu}}$ are larger than those in R^ν due to the smaller antineutrino flux, so that the measurement of ρ is dominated by statistical error.

We estimate the experimental systematic and theoretical systematic errors in ρ to be ± 0.004 and ± 0.011 respectively with the radius-dependent E_{had} cut, and to be ± 0.010 and ± 0.012 without this cut. Because the error in ρ is dominated by the low antineutrino statistics, the total error obtained by fitting without the E_{had} cut is somewhat smaller due to the higher statistics, and this method therefore gives our best measurement of ρ .

Summary of results

Within the context of the standard model, $\rho=1$ and the neutral current interaction depends on the single parameter $\sin^2\theta_W$. Our best determination of $\sin^2\theta_W$ was obtained from fitting $\sin^2\theta_W$ to (1) with $\rho=1$, using all beam settings and energy bands, and cutting events with large E_{had} . This gave

$$\sin^2\theta_W = 0.239 \pm 0.008 \pm 0.006 \pm 0.006$$

with $E_{\text{had}} \leq E_{\text{had}}^{\text{cut}}(r)$. (11)

The first error is due to experimental statistics, the second is experimental systematics, and the third is the theoretical error. Adding all three errors in quadrature gives a total error of ± 0.011 .

The same analysis but without the cut at large E_{had} gives almost the same result, but with a larger systematic error:

$$\sin^2\theta_W = 0.238 \pm 0.006 \pm 0.011 \pm 0.006$$

with no cut at large E_{had} . (12)

Adding the three errors in quadrature gives a total error of ± 0.014 .

These values are in good agreement with the most recent results obtained from UA1 [13] and UA2 [14], calculated from the ratio M_W/M_Z , which gives $\sin^2\theta_W = 0.232 \pm 0.008$. They are also consistent with similar measurements in deep-inelastic neutrino experiments [11, 15–17].

We have obtained ρ from this data by simultaneously fitting both ρ and $\sin^2\theta_W$ using (1) and (2). This provides a good test of the Standard Model, which requires $\rho=1$. Because statistical errors are larger in this measurement, the most precise values are obtained by fitting without the radius-dependent E_{had} cut. This gives

$$\sin^2\theta_W = 0.234 \pm 0.018 \pm 0.016$$

and $\rho = 1.000 \pm 0.018 \pm 0.016$ (13)

where the errors are statistical and systematic respectively (and are coincidentally the same for both parameters). This measurement of ρ agrees perfectly with the Standard Model, and is consistent with other neutrino experiments and with recent collider results.

Acknowledgements. We are grateful for the assistance of the Fermilab staff, and of many individuals at our home institutions. This research was supported by grants from the National Science Foundation and the U.S. Department of Energy.

References

1. P.G. Reutens et al.: Phys. Lett. 152B (1985) 404
2. P.G. Reutens: Ph.D. Thesis, University of Chicago (1986)
3. C.H. Llewellyn Smith: Nucl Phys B228 (1983) 205
4. R. Blair et al.: Nucl. Instrum. Methods 226 (1984) 281
5. D.B. MacFarlane et al.: Z. Phys. C 26 (1984) 1; D.B. MacFarlane: Ph.D. thesis, Caltech 1984
6. A. de Rújula, R. Petronzio, A. Savoy-Navarro: Nucl. Phys. B154 (1979) 394
7. K. Lang et al.: Z. Phys. C 33 (1987) 483
8. R.M. Barnett: Phys. Rev. Lett. 36 (1976) 1163
9. A. Sirlin, W.J. Marciano: Nucl. Phys. B189 (1981) 442
10. D.C. Carey, K.L. Brown, C. Iselin: Decay Turtle, SLAC-246, 1982
11. H. Abramowicz et al.: Z. Phys. C 28 (1985) 51
12. We have benefitted from discussions with A. DeRujula, A. Sirlin, and E. Paschos concerning uncertainties in radiative corrections
13. G. Arnison et al.: Phys. Lett. 166B 484 (1986)
14. R. Ansari et al.: Phys. Lett. 186B 440 (1987)
15. D. Bogert et al.: Phys. Rev. Lett. 55 1969 (1985)
16. H. Abramowicz et al.: Phys. Rev. Lett. 57 298 (1986)
17. J.V. Allaby et al.: Z. Phys. C – Particles and Fields 36 611 (1987)